Single snapshot imaging of optical properties using a single-pixel camera: a simulation study

Enagnon Aguénounon
Foudil Dadouche
Wilfried Uhring
Nicolas Ducros
Sylvain Gioux

SPIE.

Single snapshot imaging of optical properties using a single-pixel camera: a simulation study

Enagnon Aguénounon,a Foudil Dadouche,a Wilfried Uhring,a Nicolas Ducros,b and Sylvain Giouxa,*
aUniversity of Strasbourg, ICube Laboratory, Illkirch, France
bUniversity Lyon, INSA Lyon, UCBL, CNRS 5220, INSERM U1206, CREATIS, Villeurbanne, France

Abstract. We present the effects of using a single-pixel camera approach to extract optical properties with the single-snapshot spatial frequency-domain imaging method. We acquired images of a human hand for spatial frequencies ranging from 0.1 to 0.4 mm^{-1} with increasing compression ratios using adaptive basis scan wavelet prediction strategy. In summary, our findings indicate that the extracted optical properties remained usable up to 99% of compression rate at a spatial frequency of 0.2 mm^{-1} with errors of 5% in reduced scattering and 10% in absorption. © The Authors. Published by SPIE under a Creative Commons Attribution 4.0 Unported License. Distribution or reproduction of this work in whole or in part requires full attribution of the original publication, including its DOI. [DOI: 10.1117/1.JBO.24.7.071612]

1 Introduction

Over the last decade, extensive progress has been made in diffuse optics toward developing quantitative, wide field, rapid, and inexpensive methods to visualize the physiological properties of living tissues. Among the numerous approaches proposed in this direction, the most recent ones rely on the spatial modulation of the light and processing in the frequency domain.[1–3] Spatial frequency-domain imaging (SFDI) techniques allow the measurement of tissues absorption and reduced scattering optical properties over an entire image at once, which are used to retrieve physiological tissues parameters.[4–10] However, major limitations of such imaging system include the necessity to project several patterns of light and to illuminate sequentially at several wavelengths to extract physiological parameters, impeding the use of such technology for real-time imaging.

To increase the speed of acquisition, some approaches have proposed to reduce the number of projected patterns.[11–14] Methods, such as single-snapshot imaging of optical properties (SSOP), make use of a single pattern of light,[11,12] and the combination of this method with temporal encoding of the wavelengths has been proposed to achieve rapid multispectral acquisitions.[15,16] However, these approaches still make use of standard camera-based technology such as complementary metal–oxide–semiconductor (CMOS) or charge-coupled device (CCD) sensors that are generally expensive, monochromatic, limited in dynamic range, and importantly are limiting for multi- and hyperspectral imaging configurations.

In front of these limitations, compressive optics is a promising alternative to conventional imaging for diffuse optics. In particular, single-pixel cameras (SPCs) exhibit increased sensitivity and higher dynamic range due to efficient electronic designed for high-end photodiode or single-photon detector,[17] as well as low-cost multispectral imaging capabilities.[18–21]

In this paper, we explore numerically, using real SSOP data, the possibilities and limitations offered by compressive optics for real-time implementation using SSOP associated to an SPC (Fig. 1). In particular, we compressed existing SSOP data using compressive optics algorithms to evaluate the accuracy in extracting optical properties and the theoretical acquisition time required as a function of the compression rate of the SPC acquisition.

2 Materials and Methods

2.1 Single-Snapshot Imaging of Optical Properties

The standard SFDI method requires to acquire several images of the scene sequentially at two different spatial frequencies (e.g., $f_x = 0$ and 0.2 mm^{-1}) and three different phases (0 deg, 120 deg, and 240 deg) to obtain the modulation amplitude of each spatial frequency.[3] In comparison, the SSOP method requires the acquisition of a single image and relies on filtering in the Fourier domain to extract the amplitude modulation at two spatial frequencies: $f_x = 0$ mm^{-1} and the projected spatial frequency (e.g., $f_x = 0.2$ mm^{-1}). From these measurements, diffuse reflectances at these spatial frequencies are obtained by calibration using a phantom with known optical properties.[3] The measured diffuse reflectances allow to extract the absorption as well as the reduced scattering properties from a precomputed look-up table.[24,25]

2.2 Compressed Sensing

An SPC is an experimental setup that can measure the dot product of a scene and some user-defined pattern. See Ref. 26 for a review of this approach. The key idea is to acquire by hardware a compressed version of the scene by measuring

$$\mathrm{m} = \mathbf{h}^T \mathbf{p}, \qquad (1)$$

where $\mathbf{h} \in \mathbb{R}^{N^2}$ represents the image of the scene, $\mathbf{p} \in \mathbb{R}^{N^2}$ represents the pattern that is loaded on the spatial light modulator, and N^2 denotes the number of pixels of the spatial light modulator.

The image $\mathbf{h}$ can be recovered by postprocessing a collection of measurements $\{m_i\}$, $1 \leq i \leq I$, obtained for different patterns $\{p_i\}$, where I represents the number of patterns. Let $\mathbf{m} = [m_1, \cdots, m_I]^T$ be the measurement vector and
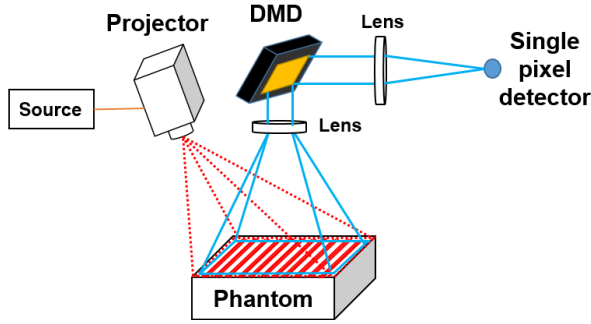
Fig. 1 Schematics of a possible implementation of an SSOP imaging system associated to an SPC (SSOP-SPC).[18,21–23] A custom single pattern projector consisting of a printed pattern on transparent substrate and an objective lens could be used on the projection side. On the detection side, a single DMD board (Vialux V7000-VIS) along with coupling optics (achromatic doublet lenses or objective lenses Vialux STAR-07) to image the scene on the DMD and collect the signal onto a single-pixel detector (DET100A, Thorlabs).

$\mathbf{P} = [\mathbf{p}_1, \cdots, \mathbf{p}_I]^T$ be the measured patterns. Assuming that the measurement vector is a compressed version of the scene, we estimate the scene by the least-squares method:

$$\mathbf{h} = \mathbf{P}^T (\mathbf{P}\mathbf{P}^T)^{-1} \mathbf{m}, \qquad (2)$$

for which fast implementations are available.[27] In this paper, we choose the patterns as Daubechie wavelets with four vanishing moments, which is a common choice in image compression.[27] The wavelet patterns to acquire are determined iteratively during acquisition according to the adaptive basis scan wavelet prediction strategy described in Ref. 28.

The number of pattern I is an acquisition parameter. Large numbers of patterns lead to high image quality but long acquisitions. We define the acquisition compression ratio (in %) as:

$$cr = \left(1 - \frac{I}{N^2}\right) \times 100. \qquad (3)$$

2.3 Data Processing and Results Analysis

To evaluate the performances of an SSOP-SPC system, we acquired a set of hand images at multiple spatial frequencies ($f_x = 0$, 0.1, 0.2, 0.3, and 0.4 mm^{-1}) at a wavelength of 665 nm and three evenly distributed phases (SFDI acquisition).[29] This range of spatial frequencies was chosen for investigating the trade-off between compression ratio and image quality, in the context of SSOP-SPC.[30] Then, we compressed a single-phase image from the set of images acquired with SFDI to simulate the acquisition of a single SSOP image by an SPC, with increasing compression ratios of 0%, 50%, 90%, 98%, 99%, and 99.5% using the adaptive basic scan described above with $N = 1024$. The resulting images are shown in Fig. 2. Each of the simulated SSOP-SPC images was then processed using the SSOP method to extract the absorption and reduced scattering maps.

The SSOP-SPC approach was evaluated by comparing the absorption and reduced scattering maps recovered from the original SFDI images and from the SSOP-SPC images. This comparison was done by measuring the mean percentage error in absorption and reduced scattering over a 400×350 pixels region of interest (see Fig. 3) given by the following equation:

$$\text{Error \%} = \frac{1}{N \times M} \sum_{n=0}^{N-1} \sum_{m=0}^{M-1} \left| 100 \times \frac{(\mu_{n,m}^{\text{SFDI}} - \mu_{n,m}^{\text{SSOP}})}{\mu_{n,m}^{\text{SSOP}}} \right|, \qquad (4)$$

where $N = M = 1024$ are the image pixel size and μ represents either μ_a or μ_s'. We also computed the theoretical SPC acquisition time according to:
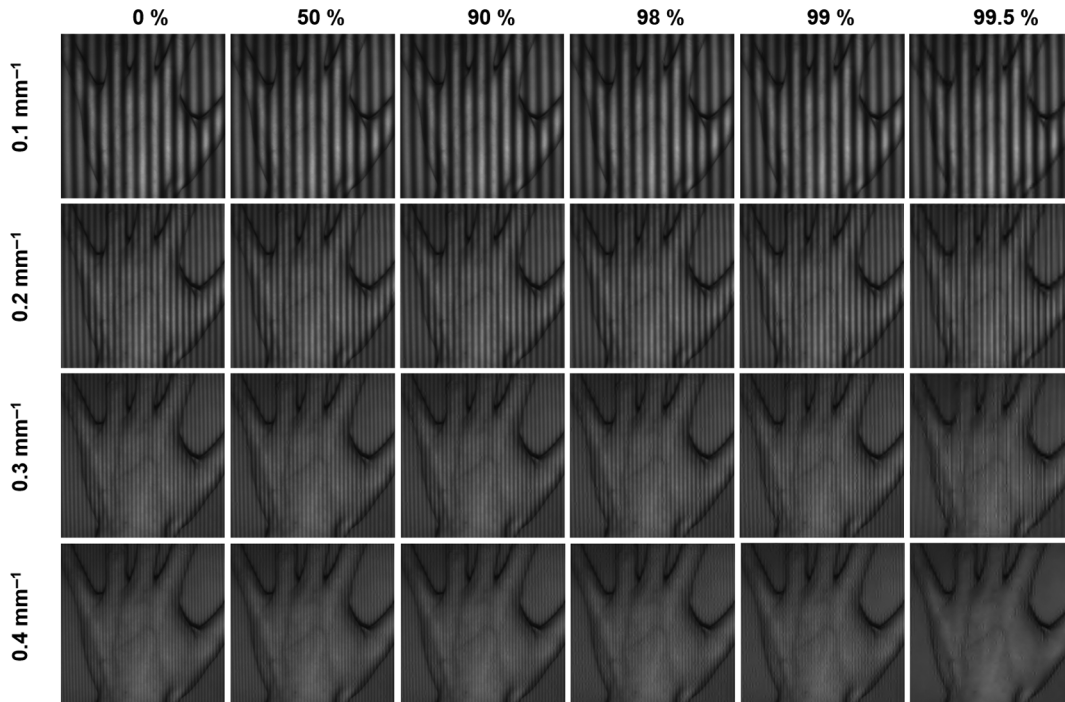

Fig. 2 SPC images acquired with an adaptive basic scan prediction strategy. Different compression ratios are displayed in different columns, and different spatial frequencies f_x are displayed in different rows.
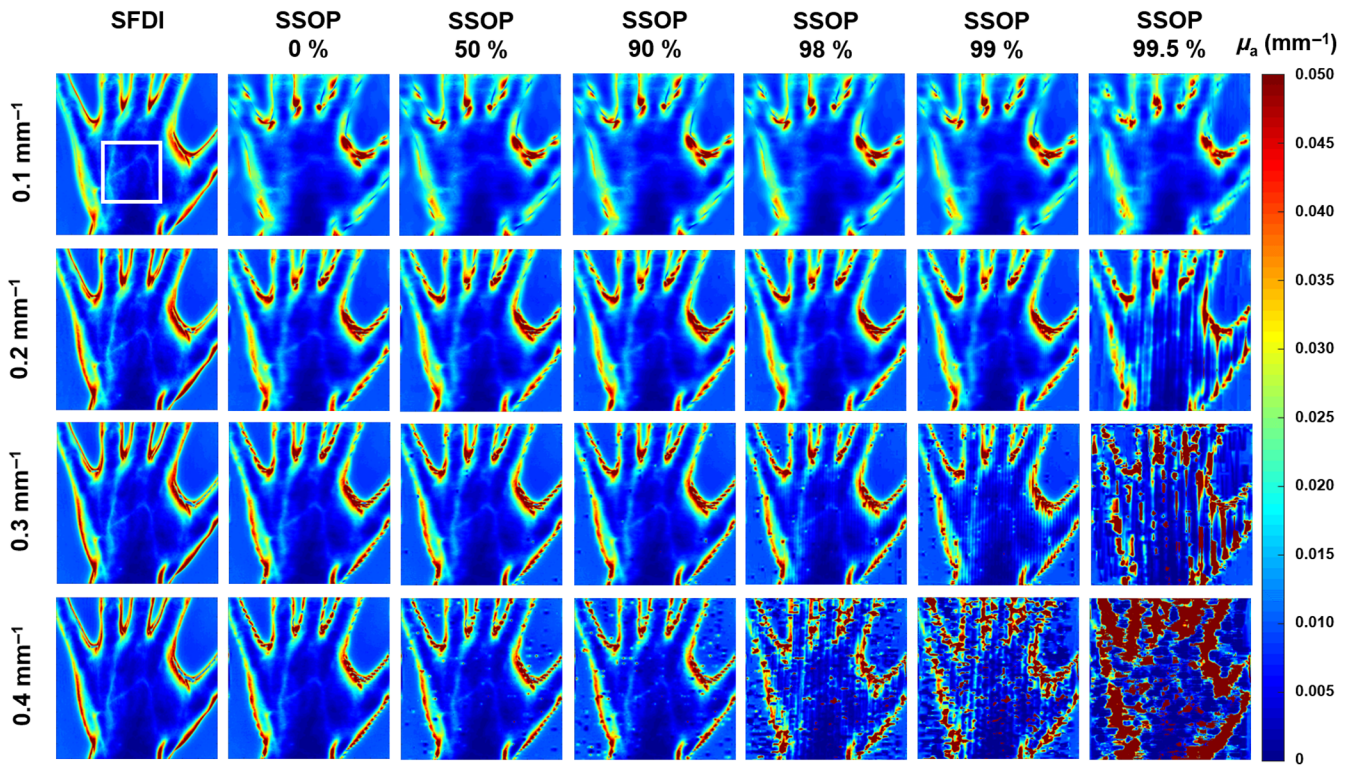
Fig. 3 Absorption map retrieved at four spatial frequencies with SFDI (first column), and SSOP for compressed images. Different compression ratios are displayed in different columns, and different spatial frequencies f_x are displayed in different rows. The region of interest used for analysis is indicated in white on the top left image.
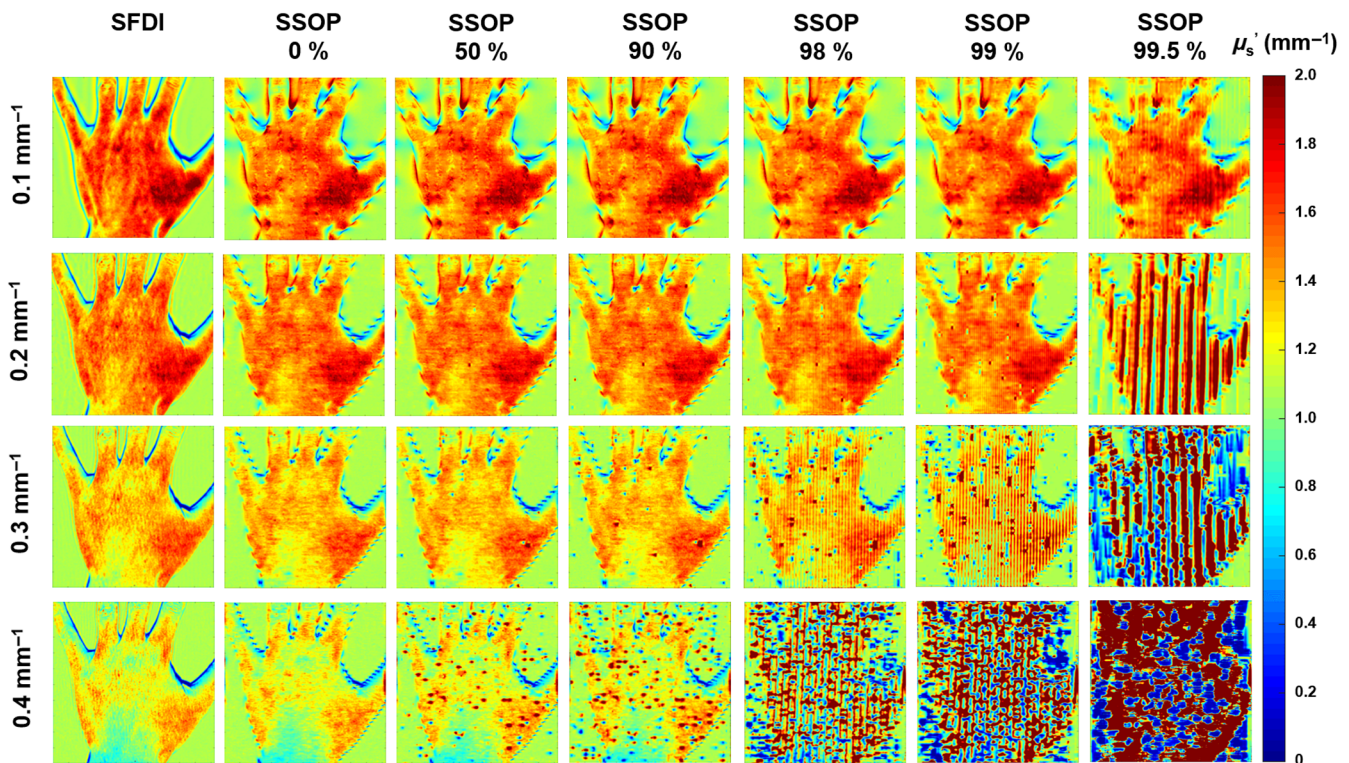

Fig. 4 Reduced scattering map retrieved at four spatial frequencies with SFDI (first column), and SSOP for compressed images. Different compression ratios are displayed in different columns, and different spatial frequencies f_x are displayed in different rows.

$$\text{Time (in ms)} = \frac{N \times M}{f_{\text{DMD}}} \times \left(1 - \frac{\text{cr}}{100}\right), \qquad (5)$$

where f_{DMD} (in kHz) represents the digital micromirror device refresh rate, set to 20 kHz.

3 Results

The results of the absorption and reduced scattering coefficient recovered by the SFDI method and by the SSOP-SPC method at the different compression rates are shown in Figs. 3 and 4, respectively. These figures make it possible to visually assess the qualitative degradation of the images extracted based on different compression rates and the change in reduced scattering due to the more superficial measurement when the spatial frequency is increasing.

Results quantifying the mean and standard deviation percentage error in absorption and reduced scattering are presented in Tables 1 and 2, respectively. These tables show the average percent error based on the compression rate at each spatial frequency projected. Bold values are the results similar to the SFDI reference measurement. Overall, good results (i.e., without major difference in errors compared to the 0% compression rate results) can be obtained with 99.5% compression rate at 0.1 mm^{-1}, 99% compression rate at 0.2 mm^{-1}, and 90% compression rate at 0.3 mm^{-1}. The method is not usable without significant inaccuracies for 0.4 mm^{-1}.

These tables also shows that best overall performances indicated by the lowest mean percentage error are obtained with a spatial frequency of 0.3 mm^{-1}. Overall, the bold values show almost constant mean percentage error for one given spatial frequency that could be used to perform SSOP imaging with an SPC.

Results of minimum theoretical acquisition time are reported in Table 3 using a 20-kHz DMD with a single photodetector

Table 1 Mean and standard deviation percentage error in absorption.

		Compression rate					
		0%	50%	90%	98%	99%	99.5%
Spatial frequency	0.1 mm^{-1}	**16.2 ± 12.9**	**16.2 ± 12.9**	**16.2 ± 12.9**	**16.2 ± 12.8**	**16.1 ± 12.8**	**15.8 ± 12.7**
	0.2 mm^{-1}	**9.6 ± 7.5**	**9.6 ± 7.6**	**9.6 ± 7.6**	**9.7 ± 7.6**	**10.1 ± 8.1**	34.1 ± 28.7
	0.3 mm^{-1}	**7.3 ± 5.8**	**7.4 ± 6.1**	**7.8 ± 7.5**	10.8 ± 11.6	16.8 ± 14.9	58.7 ± 30.6
	0.4 mm^{-1}	**8.0 ± 6.4**	9.6 ± 10.2	12.2 ± 13.5	36.9 ± 29.2	54.3 ± 32.7	70.3 ± 31.4

Note: Bold values are the results similar to the SFDI reference measurement.

Table 2 Mean and standard deviation percentage error in reduced scattering.

		Compression rate					
		0%	50%	90%	98%	99%	99.5%
Spatial frequency	0.1 mm^{-1}	**5.8 ± 4.3**	**5.8 ± 4.3**	**5.8 ± 4.3**	**5.7 ± 4.3**	**5.7 ± 4.3**	**6.0 ± 4.6**
	0.2 mm^{-1}	**3.9 ± 3.2**	**4.0 ± 3.7**	**4.0 ± 3.7**	**4.1 ± 3.7**	**4.9 ± 5.3**	33.1 ± 30.3
	0.3 mm^{-1}	**4.2 ± 3.4**	**4.3 ± 4.0**	**4.8 ± 6.6**	9.2 ± 11.5	16.7 ± 15.5	58.1 ± 31.2
	0.4 mm^{-1}	**6.0 ± 4.8**	8.2 ± 10.4	10.9 ± 14.3	38.4 ± 30.1	55.9 ± 33.1	71.7 ± 31.3

Note: Bold values are the results similar to the SFDI reference measurement.

Table 3 Minimum theoretical acquisition time in second.

		Compression rate					
		0%	50%	90%	98%	99%	99.5%
Spatial frequency	0.1 mm^{-1}	**52.43**	**26.21**	**5.24**	**1.05**	**0.52**	**0.26**
	0.2 mm^{-1}	**52.43**	**26.21**	**5.24**	**1.05**	**0.52**	0.26
	0.3 mm^{-1}	**52.43**	**26.21**	**5.24**	1.05	0.52	0.26
	0.4 mm^{-1}	**52.43**	26.21	5.24	1.05	0.52	0.26

Note: Bold values are the results similar to the SFDI reference measurement.

synchronized with the DMD refresh rate (i.e., acquisition time of 50 μs). Logically, acquisition time decreases with compression rate and is not dependent on the spatial frequency of patterns projected on the scene. In summary, best overall performance in both acquisition time and accuracy, shown in bold fonts, are obtained at 99% compression rate with 0.2 mm^{-1} and a resulting acquisition time 520 ms.

4 Discussion

In this study, we evaluated the potential of using an SPC in an SSOP system. To this end, images were acquired on an experimental SFDI system at different spatial frequencies and compressed at different compression rates according to the adaptive basis scan wavelet prediction strategy. These images were then processed using the SSOP processing method to extract their optical properties. Finally, these results were compared to the SFDI processing results on the original images.

In summary, this study shows that at spatial frequencies of 0.1 and 0.2 mm^{-1} optical properties can be extracted accurately with a 99% compression rate resulting in a 520-ms theoretical acquisition time. When adding the constraint for a good quality image, SSOP-SPC imaging can be performed optimally at 0.2 mm^{-1} with a compression rate of 99%. At higher spatial frequencies, while better precision in extracting optical properties and improved image quality can be obtained at low compression rates, degradations at higher compression rates significantly impacts the precision of the extracted optical properties, limiting its potential for fast imaging.

This study highlights the trade-off that exists between the choice of the spatial frequency used for acquisition and the capacity for the SSOP-SPC method to perform in real time. As evidenced through the results, the choice of the spatial frequency has naturally a direct consequence on the image quality when using SSOP. Decreasing spatial frequency in SSOP-SPC allows faster acquisition but results in image degradation.[30]

This study reveals that more technological progress is necessary for using SSOP with an SPC in real time. Using the current technology (20-kHz DMD), 520-ms acquisition time is obtained at 99% compression rate when a scientific CMOS camera can reach up to 200 frames per second (i.e., 5-ms acquisition time), nearly a 100-fold difference. In addition, at a spatial frequency of 0.3 mm^{-1}, where best precision is obtained, it would take 5.24 s of acquisition time at 90% of compression rate. It is clear that faster spatial light modulator technology is required to be able to use the SSOP-SPC method in real time.

Despite this limitation, it is important to remember a few points. First, an SPC is potentially more sensitive than the conventional CMOS or CCD cameras in the near-infrared, a wavelength band that is regularly used in diffuse optics. It will, therefore, not be necessary to increase the exposure time as much as with a conventional camera. Second, the main interest in using a single-pixel architecture is the potential for multi- or hyperspectral measurements. Current SFDI hyperspectral measurements typically require tunable filters, filter wheel, and sequential acquisition on a single camera or a hyperspectral camera.[10,31–34] None of these technologies is either cost-effective or allows real-time measurement. A single-pixel architecture can easily scale to several wavelengths by replacing the photosensor in SPC with line array of photosensors.

5 Conclusion

In this paper, we explore the possibilities and limitations offered by compressive optics for real-time implementation using SSOP associated to an SPC. In particular, we evaluate the accuracy in extracting optical properties and the theoretical acquisition time required as a function of the compression rate of the SPC acquisition. The results show that usable optical properties with errors <10% in absorption and 5% in reduced scattering can be extracted at a spatial frequency of 0.2 mm^{-1} with a compression rate of 99% resulting in a 520-ms acquisition time. This work contributes to the exploration of the benefits of SPC in the development of diffuse optical imaging.

References

1. N. Dognitz and G. Wagnieres, "Determination of tissue optical properties by steady-state spatial frequency-domain reflectometry," *Lasers Med. Sci.* **13**(1), 55–65 (1998).
2. D. J. Cuccia et al., "Quantitation and mapping of tissue optical properties using modulated imaging," *J. Biomed. Opt.* **14**(2), 024012 (2009).
3. J. P. Angelo et al., "Review of structured light in diffuse optical imaging," *J. Biomed. Opt.* **24**(7), 071602 (2018).
4. A. Mazhar et al., "Spatial frequency domain imaging of port wine stain biochemical composition in response to laser therapy: a pilot study," *Lasers Surg. Med.* **44**(8), 611–621 (2012).
5. A. M. Laughney et al., "Spectral discrimination of breast pathologies in situ using spatial frequency domain imaging," *Breast Cancer Res.* **15**(4), R61 (2013).
6. J. T. Nguyen et al., "A novel pilot study using spatial frequency domain imaging to assess oxygenation of perforator flaps during reconstructive breast surgery," *Ann. Plast. Surg.* **71**(3), 308–315 (2013).
7. U. Sunar et al., "Quantification of PpIX concentration in basal cell carcinoma and squamous cell carcinoma models using spatial frequency domain imaging," *Biomed. Opt. Express* **4**(4), 531–537 (2013).
8. D. M. McClatchy, III et al., "Wide-field quantitative imaging of tissue microstructure using sub-diffuse spatial frequency domain imaging," *Optica* **3**(6), 613–621 (2016).
9. S. Nandy et al., "Characterizing optical properties and spatial heterogeneity of human ovarian tissue using spatial frequency domain imaging," *J. Biomed. Opt.* **21**(10), 101402 (2016).
10. M. Ghijsen et al., "Quantitative real-time optical imaging of the tissue metabolic rate of oxygen consumption," *J. Biomed. Opt.* **23**(3), 036013 (2018).
11. J. Vervandier and S. Gioux, "Single snapshot imaging of optical properties," *Biomed. Opt. Express* **4**(12), 2938–2944 (2013).
12. M. van de Giessen, J. P. Angelo, and S. Gioux, "Real-time, profile-corrected single snapshot imaging of optical properties," *Biomed. Opt. Express* **6**(10), 4051–4062 (2015).
13. K. P. Nadeau, A. J. Durkin, and B. J. Tromberg, "Advanced demodulation technique for the extraction of tissue optical properties and structural orientation contrast in the spatial frequency domain," *J. Biomed. Opt.* **19**(5), 056013 (2014).
14. Z. R. Hoffman and C. A. DiMarzio, "Single-image structured illumination using Hilbert transform demodulation," *J. Biomed. Opt.* **22**(5), 056011 (2017).

15. M. B. Applegate and D. Roblyer, "High-speed spatial frequency domain imaging with temporally modulated light," *J. Biomed. Opt.* **22**(7), 076019 (2017).
16. E. Aguenounon et al., "Real time hyperspectral imaging using high frame rate video camera and GPGPU processing," in *SIGNAL, Third Int. Conf. Adv. Signal, Image and Video Process.*, Nice, France (2018).
17. R. H. Hadfield, "Single-photon detectors for optical quantum information applications," *Nat. Photonics* **3**(12), 696–705 (2009).
18. M. Torabzadeh et al., "Compressed single pixel imaging in the spatial frequency domain," *J. Biomed. Opt.* **22**(3), 030501 (2017).
19. A. Farina et al., "Multiple-view diffuse optical tomography system based on time-domain compressive measurements," *Opt. Lett.* **42**(14), 2822–2825 (2017).
20. Q. Pian, R. Y. Yao, and X. Intes, "Hyperspectral wide-field time domain single-pixel diffuse optical tomography platform," *Biomed. Opt. Express* **9**(12), 6258–6272 (2018).
21. F. Rousset et al., "Time-resolved multispectral imaging based on an adaptive single-pixel camera," *Opt. Express* **26**(8), 10550–10558 (2018).
22. S. Belanger et al., "Real-time diffuse optical tomography based on structured illumination," *J. Biomed. Opt.* **15**(1), 016006 (2010).
23. M. Ochoa et al., "Assessing patterns for compressive fluorescence lifetime imaging," *Opt. Lett.* **43**(18), 4370–4373 (2018).
24. J. Angelo et al., "Ultrafast optical property map generation using lookup tables," *J. Biomed. Opt.* **21**(11), 110501 (2016).
25. S. Panigrahi and S. Gioux, "Machine learning approach for rapid and accurate estimation of optical properties using spatial frequency domain imaging," *J. Biomed. Opt.* **24**(7), 071606 (2018).
26. M. F. Duarte et al., "Single-pixel imaging via compressive sampling," *IEEE Signal Process. Mag.* **25**(2), 83–91 (2008).
27. I. Daubechies, *Ten Lectures on Wavelets*, Society for Industrial and Applied Mathematics, Philadelphia, Pennsylvania (1992).
28. F. Rousset et al., "Adaptive basis scan by wavelet prediction for single-pixel imaging," *IEEE Trans. Comput. Imaging* **3**(1), 36–46 (2017).
29. M. Schmidt et al., "Real-time, wide-field, and quantitative oxygenation imaging using spatiotemporal modulation of light," *J. Biomed. Opt.* **24**(7), 071610 (2019).
30. E. Aguenounon et al., "Single snapshot of optical properties image quality improvement using anisotropic 2D windows filtering," *J. Biomed. Opt.* **24**(7), 071611 (2019).
31. J. R. Weber et al., "Multispectral imaging of tissue absorption and scattering using spatial frequency domain imaging and a computed-tomography imaging spectrometer," *J. Biomed. Opt.* **16**(1), 011015 (2011).
32. S. Gioux et al., "First-in-human pilot study of a spatial frequency domain oxygenation imaging system," *J. Biomed. Opt.* **16**(8), 086015 (2011).
33. A. Mazhar et al., "Implementation of an LED-based clinical spatial frequency domain imaging system," *Proc. SPIE* **8254**, 82540A (2012).
34. M. Ghijsen et al., "Real-time simultaneous single snapshot of optical properties and blood flow using coherent spatial frequency domain imaging (cSFDI)," *Biomed. Opt. Express* **7**(3), 870–882 (2016).

Foudil Dadouche received his engineering degree from the University of Sciences and Technology of Oran, Algeria, and his electronic master's and PhD degrees from the University of Pierre and Marie Curie (Paris VI). He joined the University of Strasbourg as an associate professor in 2010. He is member of the ICube Laboratory. His main research interests include imaging systems, digital electronics, and photovoltaics.

Nicolas Ducros received his MSc in electrical engineering and MSc in biomedical engineering, both from the University of Strasbourg, France, in 2006. He obtained his PhD in electrical engineering from the University of Lyon, in 2009. After a postdoctoral fellowship at Politecnico Milan, he became an associate professor at the University of Lyon with the Biomedical Imaging Laboratory CREATIS. His research interests include image processing and inverse problems.

Biographies of the other authors are not available.